Thiede, J., Myhre, A.M., Firth, J.V., Johnson, G.L., and Ruddiman, W.F. (Eds.), 1996
Proceedings of the Ocean Drilling Program, Scientific Results, Vol. 151

28. QUATERNARY PALEOCEANOGRAPHY AND PALEOCLIMATOLOGY OF THE FRAM STRAIT/YERMAK PLATEAU REGION: EVIDENCE FROM SITES 909 AND 912[1]

Kjersti Hevrøy,[2] Gaute Lavik,[2] and Eystein Jansen[2,3]

ABSTRACT

The drilling on Leg 151 provided the first sections that allow studies beyond isotope Stage 6 in the Fram Strait/Yermak Plateau area, thereby enabling insight into paleoenvironmental evolution prior to the last glacial cycle. The upper parts of Holes 909B and 912A were analyzed for their ice-rafted detritus (IRD) and foraminiferal contents and stable isotope compositions to obtain a relatively high-resolution record of the paleoenvironmental evolution during the last 400 k.y. in the region. The main features are similar to the records from the Fram Strait and the Yermak Plateau. Earlier glaciations (isotope Stages 6–12) were more severe than the last one. The content of foraminifers through time indicates a trend toward more open water, with a higher production through the two last glacial/interglacial cycles. Seasonal open-water conditions with a high foraminifer production occurred through all the glacial periods, indicating that the surface circulation of the Nordic Seas in glacial stages plays an important role in the growth and decay of high-latitude ice sheets, bringing moisture and heat northward during the glacials. Deep-water formation seems to be continuous in the Nordic Seas through most of the time period presented in this study. There was an apparent change in the style of glaciation in the earlier parts of the Brunhes Chron with the emergence of more strongly developed IRD peaks than before. Glacial activity also is an important element in the Matuyama Chron in the European Arctic.

INTRODUCTION

The Fram Strait and Yermak Plateau region is an important area for the exchange of water and energy between the Arctic Ocean and the Nordic Seas. We studied Hole 909B (78°35.07′N, 3°4.38′E; 2519 m water depth) in the Fram Strait and Hole 912A (79°57.557′N, 5°27.360′E; 1036 m water depth) on the Yermak Plateau (Fig. 1) to provide a paleoclimatic and paleoceanographic record from this area for the last few glacial/interglacial cycles, focusing on the surface and deep-water communication between the Arctic Ocean and the Nordic Seas, the influx of North Atlantic surface water to the Arctic, and variations in continental ice sheets. The study is based on planktonic and benthic isotope stratigraphy ($\delta^{18}O$ and $\delta^{13}C$), foraminifers, and the amount and composition of ice-rafted material. The Fram Strait is influenced by water masses from all the surrounding oceans—the Arctic Ocean, the Barents Sea and the Nordic Seas (Fig. 1). The surface circulation of the Fram Strait is dominated by two currents: The West Spitsbergen Current (WSC), which transports warm, saline Atlantic water northward, and the East Greenland Current (EGC), which brings cold, low-salinity polar water southward. Between these water masses is the Arctic water, which is a mixture of Atlantic and polar waters. The flow of deep water, formed in the Arctic Ocean and the Barents Sea by brine formation and by strong cooling of inflowing Atlantic water, is southward beneath the EGC. Some of the deep water formed by convection in the Greenland Sea is transported northward along the eastern Fram Strait together with some of the deep water formed in the Barents Sea.

Ocean basins at high latitudes are important for an understanding of global climate and climate changes because they directly influence global climate through the formation of permanent and seasonal sea-ice cover, the transfer of heat to the atmosphere, and the renewal and ventilation of deep water. The climate in the Arctic is strongly influenced by sea-ice cover, which increases the regional albedo and reduces the heat and gas exchange between the ocean and atmosphere. There also is a close relationship between sea-ice cover and sedimentation (Hebbeln and Wefer, 1991). The location of these cores is within the marginal zone of the sea-ice cover and close to the northernmost extension of the WSC (Fig. 1). The sea-ice cover varies seasonally and interanually, and, because of these variations, this area is well suited for studies of the relation between ice cover, sedimentation, and circulation.

Previous studies have shown that the ocean circulation of this region has changed through the last glacial cycles. A much more extensive sea-ice cover has been proposed for the last glacial, with a dominating current of cold, polar water moving southward through the Fram Strait (Kellogg, 1980). CLIMAP reconstructions of the last glacial maximum suggest that there was a perennial sea-ice cover in the Nordic Seas with only an isolated circulation cell in the Greenland Sea (CLIMAP Project Members, 1976; Kellogg, 1980). Terrestrial data from northern Norway indicate seasonal open waters (Vorren et al., 1988), and an influx of Atlantic waters as far north as the Fram Strait has been indicated recently (Dokken, 1995; Hebbeln et al., 1994). This may imply that a northward heat flux from open waters and its effects on atmospheric circulation may have been important factors for the rapid growth of high-latitude ice sheets. Previous work in these northern regions mostly concentrated on the last glacial/interglacial cycle; little is known on glacial variability beyond the last two glacial/interglacial cycles. The drilling on Leg 151 provided the first sections that allow studies of paleoenvironments predating isotope Stage 6 in this region, thereby enabling insight into paleoenvironmental evolution prior to the last glacial cycle.

MATERIALS AND METHODS

Hole 909B was cored to 135.1 mbsf, and Hole 912A was cored to 145.4 mbsf. The work presented here covers the upper 20 m and 15 m of these cores, respectively. The sediments are mainly dark gray, nonlithified, slightly to moderately bioturbated silty clay and clayey silt. There are small visual variations through the sections. At the break between Cores 2H and 3H, in both Holes 909B and 912A, there are overlapping core-log depths due to more than 100% recovery. These have been adjusted slightly to avoid the overlaps.

[1]Thiede, J., Myhre, A.M., Firth, J.V., Johnson, G.L., and Ruddiman, W.F. (Eds.), 1996. *Proc. ODP, Sci. Results,* 151: College Station, TX (Ocean Drilling Program).

[2]Department of Geology, University of Bergen, Allégaten 41, N-5007 Bergen, Norway.
[3]Correspondence author: eystein.jansen@geol.uib.no

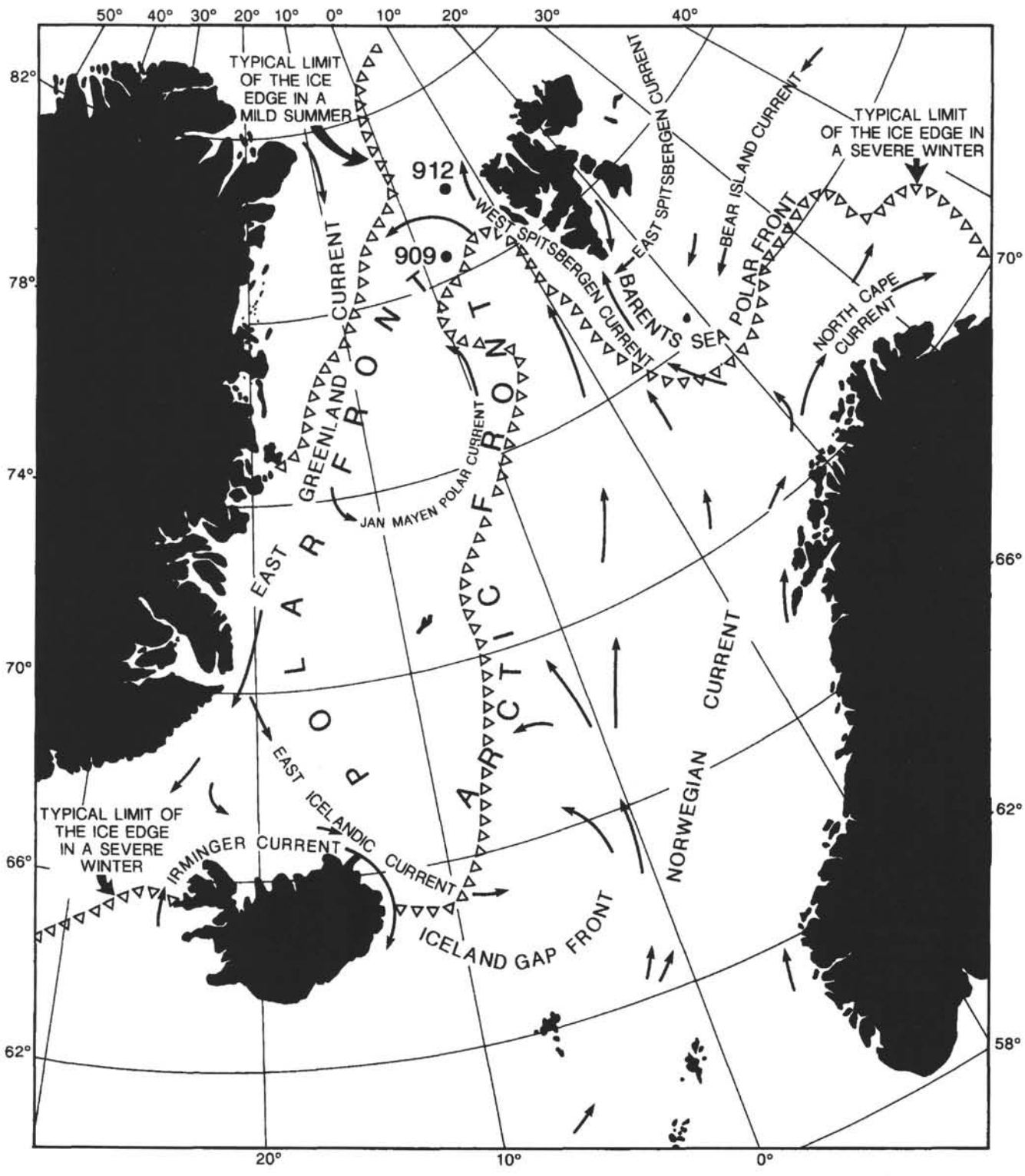

Figure 1. Location map of the investigated sites and surface currents and oceanic fronts of the present ocean.

We analyzed 10-cm^3 samples at 10-cm intervals from Hole 909B and 5-cm^3 samples at 10-cm intervals from Hole 912A. The samples were wet sieved in the fractions <63 µm, 63–125 µm, 125–1000 µm, and >1000 µm, and then dried and weighed. The 125- to 1000-µm fraction was dry sieved on a 150-µm sieve, and counting of biogenic and minerogenic (IRD) material was done on the 150- to 1000-µm fraction. Due to the dominance (>90%) of *Neogloboquadrina pachyderma* (sinistrally coiling), 1000 specimens of planktonic foraminifers were normally counted to get a better statistical reliability. In addition, minerogenic material was counted and classified in the 500- to 1000-µm fraction. The material in this fraction was divided into the following groups: monocrystalline fragments (quartz and feldspar),

sedimentary rocks (sand-, silt-, and mudstones/shales), metamorphic and crystalline rocks, coal and detrital carbonate. Samples with more than 20 grains were included in the results.

Stable isotope analyses were performed on a Finnigan MAT 251 mass spectrometer on the GMS-laboratory at the University of Bergen. Foraminiferal samples were crushed, cleaned with methanol in an ultrasonic bath, and reacted with orthophosphoric acid at 70°C on an automated carbonate preparation line using individual acid bath ("Kiel Device"). The reproducibility of the system based on replicate carbonate powder standards is 0.06‰ and 0.07‰ for $\delta^{13}C$ and $\delta^{18}O$, respectively. The planktonic isotopes are measured on *N. pachyderma* (sinistrally coiling). In Hole 909B, benthic isotopes were measured on *Cibicides wuellerstorfi* and *Oridorsalis umbonatus*. The $\delta^{18}O$ values were corrected by +0.64‰ for *C. wuellerstorfi* and +0.4‰ for *O. umbonatus* (Graham et al., 1981). In Hole 912A, the benthic species *Cassidulina teretis, Islandiella nocrossa,* and *Nonion barleeanum* were measured. *C. teretis* is believed to secrete its shell close to oxygen isotopic equilibrium (Jansen and Sejrup, 1987) and is not corrected. *I. nocrossa* values were corrected by –0.25‰, and *N. barleeanum* values were corrected by +0.16‰ (Poole et al., in press). Some samples were measured twice to check the robustness of spikes in the record.

CHRONOLOGY

The chronology of the cores is primarily based on isotope stratigraphy. In Hole 909B, the chronology is based both on oxygen and carbon isotopes, whereas in Hole 912A it is primarily based on oxygen isotopes because the carbon isotopic record deviates substantially from the normal records of the Nordic Seas and is difficult to interpret. At these high latitudes, meltwater and water mass variability significantly influence the oxygen isotopic composition of surface and deep waters, influencing both benthic and planktonic records. Thus, the isotope stratigraphy from this region is difficult to correlate in detail to the standard oxygen isotope stratigraphy. It is, however, possible to correlate the records to other deep-sea cores further south in the Nordic Seas (e.g., Vogelsang, 1990) that provide a bridge to the global oxygen isotope record. Another problem is the variable occurrence of foraminifers. Several intervals of the isotope record have low resolution due to samples barren of foraminifers, especially in the lower parts of the section. Therefore, it is necessary to use other parameters, such as the amount of ice-rafted material and the occurrence of coal (Bischof et al., 1990), to support the interpretations and to make a more accurate chronology. These problems make the isotope stage determinations somewhat inaccurate, below Stage 5 in particular.

Hole 909B

The isotope records shown in Figure 2 document many local overprints on the oxygen isotope record, whereas the carbon isotope record conforms more with records from cores further south in the Nordic Seas. In the planktonic isotope record, isotope Stage 1 is only represented by one sample with light $\delta^{18}O$ values (Fig. 2A) and heavy $\delta^{13}C$ values (Fig. 2B). Isotope Stage 2 is clearly marked by the heavy $\delta^{18}O$ and light $\delta^{13}C$ values from 0.2 to about 1 mbsf. Figure 2 documents that Stage 2 is represented by a relatively high foraminifer content, which has previously been described from the Fram Strait for this stage (Hebbeln et al., 1994). Isotope Stage 3 is characterized by three light $\delta^{18}O$ peaks. The first one, right after the Stage 3/4 boundary, is known from several isotope records from the Norwegian Sea as isotope Event 3.3.1 (Dokken, 1995; Fronval et al., 1995; Vogelsang, 1990) and dated to around 55 ka (Martinson et al., 1987). Isotope Stage 4 shows light $\delta^{13}C$ and heavy $\delta^{18}O$ values except for a light isotope peak at about 2.5 mbsf. The marked occurrence of *C. wuellerstorfi* (Fig. 2F) in the first half of Stage 4 was documented previously in core M23398 from the southern Fram Strait by Dokken (1995). The single peak occurrence of *Pullenia bulloides* (Fig. 2F) is a marker for isotope Stage 5a in the Norwegian Sea (Haake and Pflaumann, 1989) and in the Fram Strait (Hebbeln, 1992; Dokken, 1995). Stage 5a also is marked by low $\delta^{18}O$ values and high $\delta^{13}C$ values. Stage 5c is characterized by the appearance of *C. wuellerstorfi* combined with light $\delta^{18}O$ values. The maximum negative peak of $\delta^{18}O$ in isotope Stage 5e might be lost in the core break between the last sample in Stage 6 and the first in Stage 5e. There is only one sample with a relatively light $\delta^{18}O$ value at this level, and it is not simultaneous with the occurrence of *C. wuellerstorfi* as shown in other cores from the Fram Strait. Isotope Stage 6 is well defined by overall light $\delta^{13}C$ values, relatively heavy $\delta^{18}O$ values, and high amounts of IRD. The high amount of coal in the 500-µm fraction (Fig. 3D) has been described as a marker for Stage 6 in the Fram Strait by Bischof et al. (1990). In isotope Stage 7, there are very few samples with enough foraminifers for isotope measurements. There is a clear distinction between heavy $\delta^{13}C$ values in Stage 7 and light values in Stages 6 and 8, which is common in Nordic Sea records. The lower limit of isotope Stage 8 is defined by the increase in IRD deposition and the appearance of coal. Early in this stage, there is a large light isotope peak shown both in $\delta^{18}O$ and $\delta^{13}C$ values that also was found by R. Spielhagen (pers. comm., 1994) in cores from this area. Isotope Stage 9 includes two peaks of light $\delta^{18}O$ values, which might be interpreted as Substage 9.1 and 9.3, interrupted by a cold period with high amounts of IRD (Substage 9.2). Below isotope Stage 9 (9.5 mbsf), the identification of isotope stages becomes unclear. However, two intervals from 11 to 13.5 mbsf and from 14 to 17.5 mbsf are enriched in coal and IRD and may be correlated to glacial isotope Stages 10 and 12. Based on this interpretation, Stage 12 has several meltwater pulses shown in the isotope records, or light $\delta^{18}O$ combined with light $\delta^{13}C$ values, followed by a high input of IRD. Isotope Stage 11 is difficult to recognize in any of the records presented in this work. There is a core break at 14 mbsf (Fig. 2) that is just above the last sample containing coal in Stage 12. Thus, most of the material from Stage 11 could have been lost in the core break.

The average sedimentation rate is 3.88 cm/k.y. for the interval studied (isotope Stages 1–12), which is a bit lower than the average rate of 4.75 cm/k.y. for the Brunhes (Fig. 4). The glacial periods have higher sedimentation rates than the interglacials, except for Stage 9. The lower parts of the record, particularly Stages 10 and 12, have higher sedimentation rates than the upper parts. The average sedimentation rate of the Brunhes lies between the sedimentation rates for Stages 1–6 and 10 and 12. This constrains the isotope stratigraphy, which is hard to reconcile differently without imposing quite drastic changes in sedimentation rates.

Hole 912A

Isotope Stage 1 is represented by low planktonic and benthic $\delta^{18}O$ values (Fig. 5A, C). Two peaks with light $\delta^{18}O$ show stepwise melting after the last glaciation. These meltwater pulses are also shown by two small peaks in IRD. The upper part of this stage is missing. Isotope Stage 2 is well documented by high $\delta^{18}O$ values. There are abundant foraminifers in Stage 2 (Fig. 5E, F), in accordance with the results of Hebbeln et al. (1994) from the Fram Strait and the results from Hole 909B. Isotope Stage 3 has generally lower $\delta^{18}O$ values, and it is marked by three light peaks, similar to those of Hole 909B. The placement of the Stage 3/4 boundary is based on the amount of IRD (Fig. 6C) because there are no foraminifers in this interval. There is a relatively high input of IRD at the beginning of Stage 3, as has been shown by Dokken (1995) and Fronval et al. (1995), that defines the beginning of Stage 3 in cores to the south of ODP Sites 909 and 912. Oxygen isotope values are high in isotope Stage 4, clearly shown by both planktonic and benthic records.

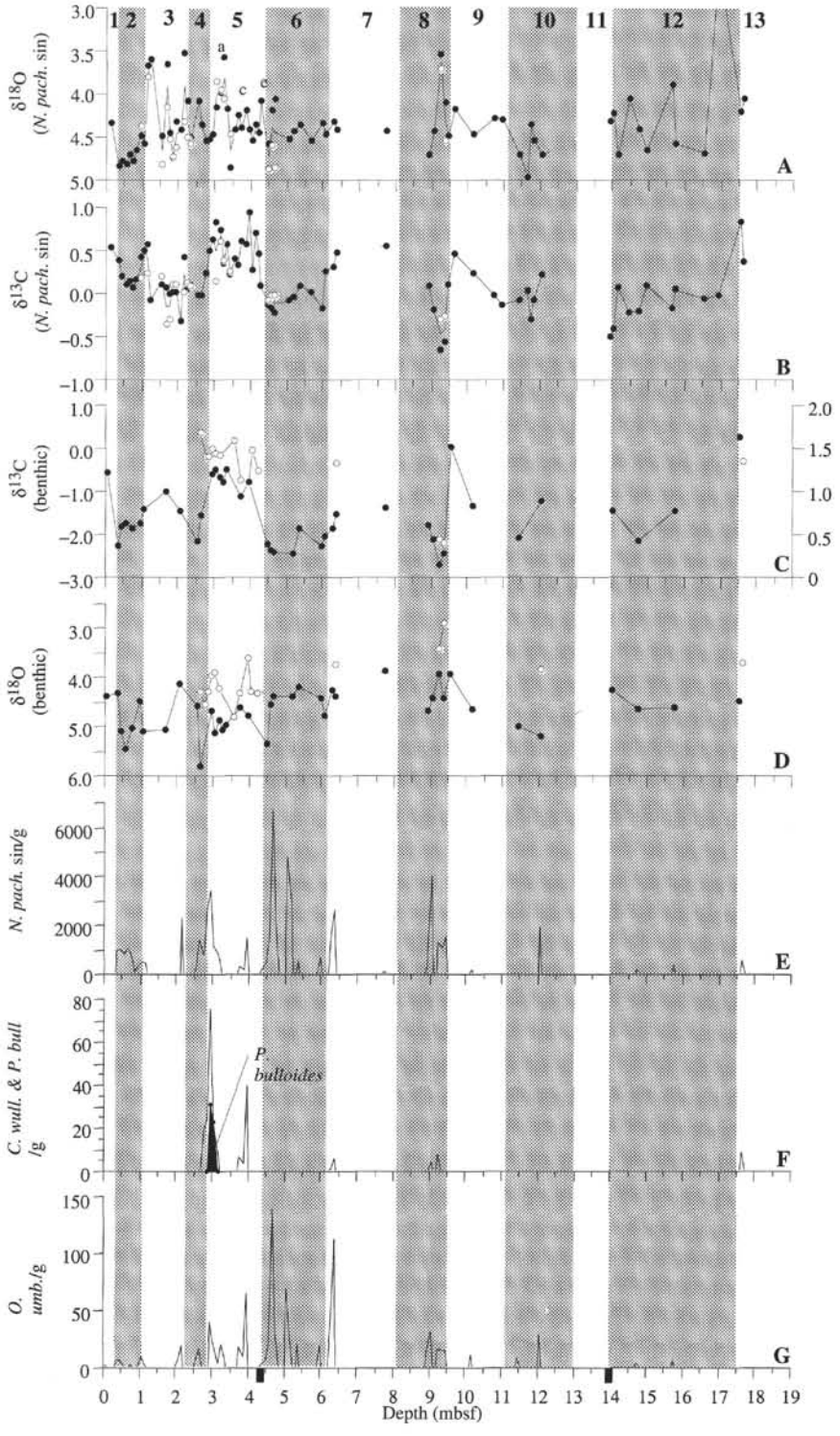

Figure 2. Isotope records in per thousand (‰) vs. PDB, and biogenic data from Hole 909B. The numbers of the isotope stages are on the top, and the glacial stages are shaded. **A.** Planktonic $\delta^{18}O$ record in per thousand (‰) vs. PDB, measured on *N. pachyderma* (sinistrally coiling). **B.** Planktonic $\delta^{13}C$ record measured on *N. pachyderma* (sinistrally coiling). Double measurements are shown by both open and solid circles in (A) and (B). **C.** Benthic $\delta^{13}C$ record from *O. umbonatus* (solid circles = left y-axis) and *C. wuellerstorfi* (open circles = right y-axis). **D.** Benthic $\delta^{18}O$ record measured on *O. umbonatus* (solid circles) and *C. wuellerstorfi* (open circles), corrected –0.4‰ and +0.63‰, respectively. **E.** Content of *N. pachyderma* (sinistrally coiling) per gram of dry sediment in the >150-µm fraction. **F.** Content of *C. wuellerstorfi* and *P. bulloides* per gram of dry sediment, based on counts in the >150-µm fraction. **G.** Content of *O. umbonatus* per gram of dry sediment, based on counts in the >150-µm fraction. Black bars on depth scale indicate core breaks.

The Stage 4/5 boundary is well developed in the $\delta^{18}O$ record, showing a clear transition from high to low values. The planktonic isotope values from isotope Stage 5 show a light early peak and relatively uniform, heavier values in the upper part. This makes it difficult to define substages in Stage 5. Ice rafting continues into Stage 5e, which is also shown by Dokken (1995) and Fronval (pers. comm., 1995) in cores to the south. The very low $\delta^{18}O$ value and high input of IRD at ~8 mbsf could, therefore, reflect a melting event at the beginning of Substage 5e.

Isotope Stage 6 is defined by high $\delta^{18}O$ values around 11 mbsf that gradually decline through the stage and culminating in a light meltwater peak. A lack of resolution may have prevented observation of the heavy upper substage of Stage 6; alternatively, there is a very long deglacial sequence at Termination II in this core. IRD is present in high amounts throughout the stage, supporting its glacial designation. The appearance of coal is a marker for Stage 6 (Bischof et al., 1990), and the coal record from Site 909 (Fig. 3D) shows that this corresponds with our definition of Stage 6. Accordingly, we have used the

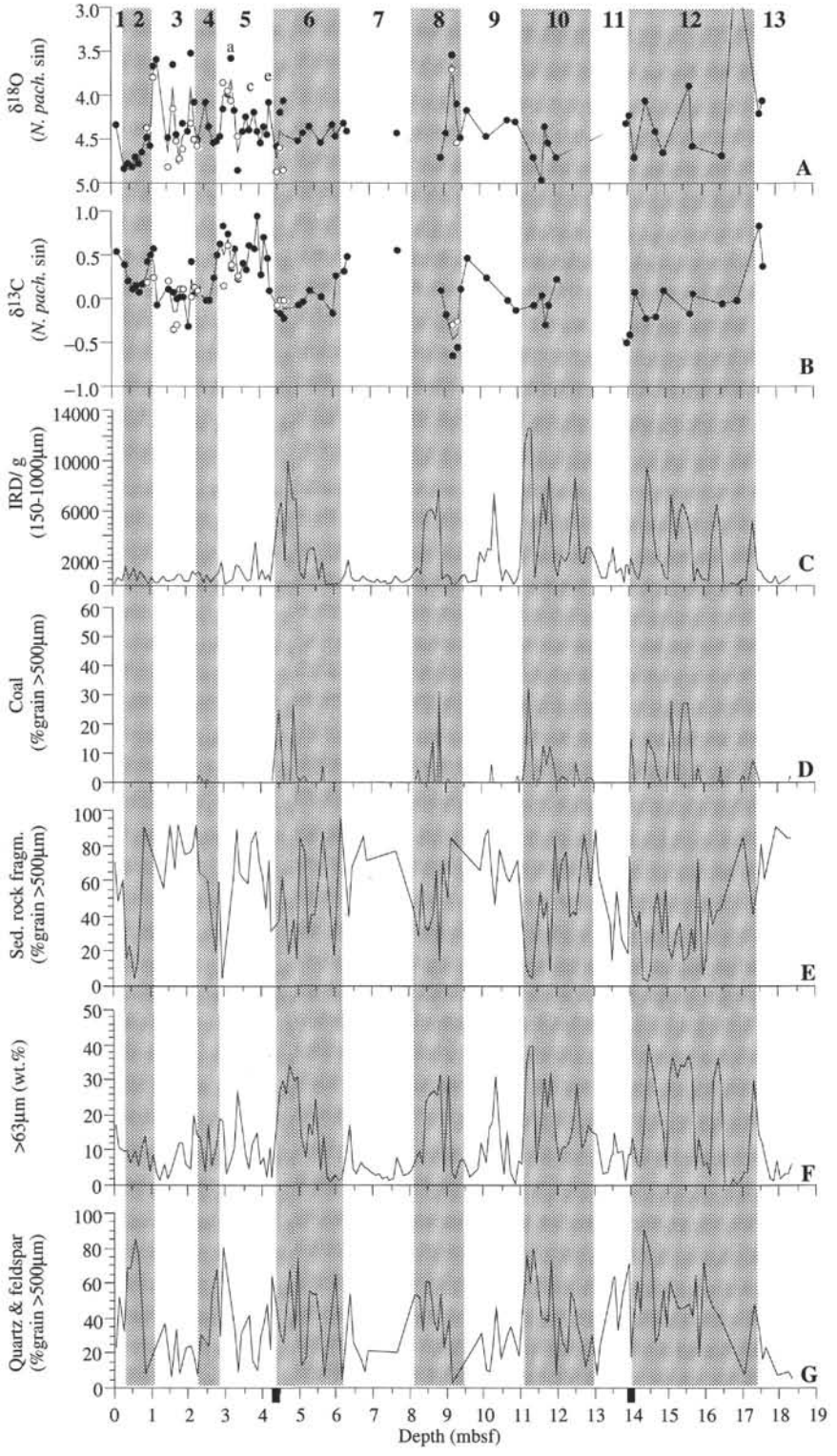

Figure 3. Planktonic isotopes in per thousand (‰) vs. PDB, and sedimentological data from Hole 909B. The numbers of the isotope stages are on top, and the cold stages are shaded. **A.** Planktonic $\delta^{18}O$ record measured on *N. pachyderma* (sinistrally coiling). **B.** Planktonic $\delta^{13}C$ record measured on *N. pachyderma* (sinistrally coiling). Double measurements are shown by both open and solid circles in (A) and (B). **C.** IRD content per gram of dry sediment, based on counts in the >150-µm fraction. **D.** Coal content in the >500-µm fraction in relative percentages, based on counts. **E.** Content of sedimentary rock fragments in relative percentages, based on counts in the >500-mm fraction. **F.** Grain size (wt% >63 µm). **G.** The content of monocrystalline rock fragments in relative percentages is based on counts in the >500-µm fraction. The black bars on depth scale indicate core breaks.

coal occurrence as additional information in defining the exact limits of the stage. Isotope Stage 7 is defined from the light $\delta^{18}O$ values.

Average sedimentation rates have been calculated for each isotope stage (Fig. 7) using the SPECMAP time scale (Martinson et al., 1987). The sedimentation rate is quite linear during the last 200 k.y., on average 6 cm/k.y. The lower part of the record has a much lower sedimentation rate of about 2.15 cm/k.y., but the chronology here is not well resolved. If we extrapolate sedimentation rates to the Brunhes/Matuyama boundary at 24.6 m, we obtain an average sedimentation rate of 2.2 cm/k.y. It seems a bit unlikely that sedimentation rates were that much lower in earlier glaciations compared to the two last ones, considering the size of the glaciations and the location of this site. The apparent lower sedimentation rates might be explained by a hiatus, possibly at about 15 mbsf, where magnetic susceptibility data

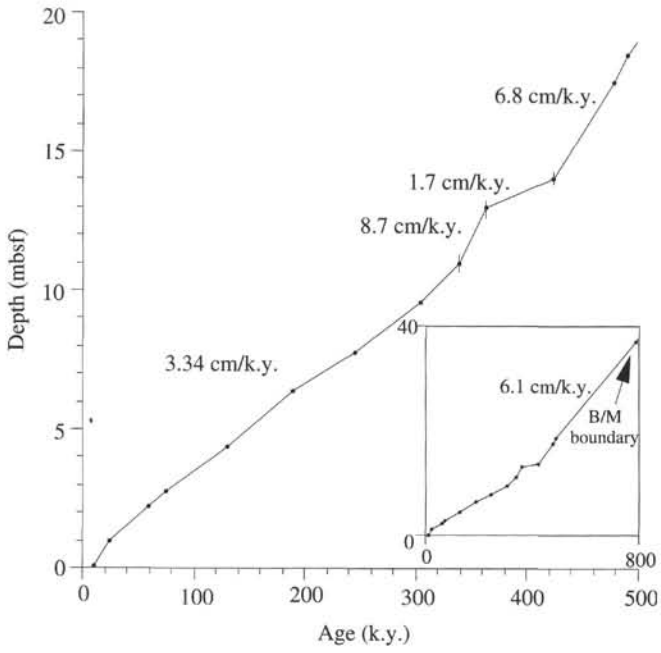

Figure 4. Average sedimentation rates in Hole 909B for the isotope stages during the last 500 k.y. Note that the period with very low sedimentation rates around 400 ka contains a core break. Sedimentation rates extending to the Brunhes/Matuyama boundary are incorporated (Myhre, Thiede, Firth, et al., 1995).

from the shipboard measurements indicate a clear shift in properties. This would give the older glaciations a higher, more likely, sedimentation rate.

RESULTS

The $\delta^{18}O$ records from Holes 909B and 912A are both very influenced by light isotope peaks that we interpret as meltwater events unrelated to sea-surface temperature (SST) increases both because they occur without signals of any SST increase high enough to make corresponding isotopic change and because the shifts are clearly beyond those related to ice-volume effect. Foraminifers are more numerous in the cold isotope stages than in the warmer stages. There are some general trends on the larger time scale that are similar in the two cores. The amounts of foraminifers, both planktonic and benthic, are much higher in the upper parts of the cores than in the lower parts. The IRD contents are higher in the glacial periods below Stage 5 than above.

Hole 909B

Isotopes and Foraminifers

Below the Stage 6/7 boundary, most of the samples are barren of foraminifers, resulting in a rather discontinuous isotope record (Fig. 2). Compared to the $\delta^{18}O$ record, which is very spiky, the $\delta^{13}C$ curve is much more conservative and seems to give a better picture of the glacial/interglacial cycles than the $\delta^{18}O$-signal. The benthic record from *O. umbonatus* shows a good covariation with the $\delta^{13}C$ record from planktonic foraminifers through most of the studied section. This is indicative of communication between the surface layer and bottom water on a general scale through the period we have studied.

Between 14 and 18 mbsf (Stage 12?), four light planktonic $\delta^{18}O$ values combined with relatively light $\delta^{13}C$ values are interpreted as meltwater pulses due to absence of warm elements in the microfossil record. The same feature occurs in Stages 8, 4, and 3. The meltwater pulse in Stage 8 is clearly shown in both the planktonic and benthic isotope records, and it is different from the other meltwater pulses that usually do not contain benthic foraminifers. In late Stage 6, replicate isotope measurements show large variability within one sample (Fig. 6A). This could be due either to measurement error, bioturbational mixing, or, perhaps more likely, to the fact that conditions are changing rapidly between meltwater events and normal, cold water in this period. In a sediment formed under rapidly changing environments, sampled in a tube with a 2-cm diameter, two levels with highly different isotopic composition could easily be mixed and provide isotopically heterogenous foraminifer populations.

C. wuellerstorfi is present through most of Stage 5, and its $\delta^{18}O$ record corresponds quite well to the planktonic record. There is a discrepancy between the $\delta^{18}O$ of *O. umbonatus* and that from *C. wullerstorfi*. This indicates that the correction values we have used based on studies further south and in other ocean basins are not accurate for this location.

C. wuellerstorfi is most abundant in the warmer stages. This is unlike *O. umbonatus* and *N. pachyderma* (sinistrally coiling), which are most abundant in the colder stages and have a very similar distribution pattern throughout the analyzed section.

IRD and Sediment Analysis

As previously mentioned, the amount of IRD is much lower than during the older glacials. Maxima of IRD are pronounced during isotope Stages 6, 8, 9, 10, and 12. A high variability in the input of IRD is typical for isotope stages below Stage 9. Large amounts of coal are recorded in all of the glacial stages downcore from Stage 5 and are only present in very small amounts in Stage 4. The amount of coal in the 500-mm fraction in the glacial stages seems to be in phase with the input of IRD (Fig. 3C, D). The more IRD there is in the 150-µm fraction, the higher the percentage of coal is in the 500-µm fraction. Also of interest is the tendency for coal fragments to be inversely correlated with the distribution of sedimentary rock fragments (Fig. 3E). Intuitively, we would expect the opposite (that coal should originate from an area with sedimentary rocks) and would, therefore, expect some covariance. Although the plots are relative percentages, we note that even for absolute content, the general trend is that sedimentary rock fragments dominate in the warmer periods with low IRD input, whereas coal and monocrystalline rock fragments dominate the colder stages. This suggests that the coal and the sedimentary rock fragments have different source areas.

The coarse fraction percentages (>63 µm) match the IRD counts from the 150-µm fraction with the exception of samples that include large amounts of foraminifers.

Both coal and planktonic foraminifers are most abundant in the glacial periods. By comparing Figures 2E and 3D in detail, it is clear, however, that the peaks of coal and foraminifers do not appear in the same samples, but are offset. This is systematic through the whole record.

Hole 912A

Isotopes and Foraminifers

The planktonic oxygen isotope record gives a good stratigraphy for this core, particularly above Stage 6 (Fig. 5A, B). The benthic isotope record has a lower resolution (Fig. 5C, D) because benthic foraminifers are absent in many intervals. The general features in the $\delta^{18}O$ record (high in glacial stages and low in interglacials and warmer periods) are the same for both records. The planktonic $\delta^{18}O$ values range from a maximum of 5‰ to a minimum of 3.1‰, and the benthic $\delta^{18}O$ values range from 5.9‰ to 4‰, which represents an amplitude of 1.9‰ for both. This shift is larger than the effect from continental ice volume and must, therefore, also reflect changes in salinity

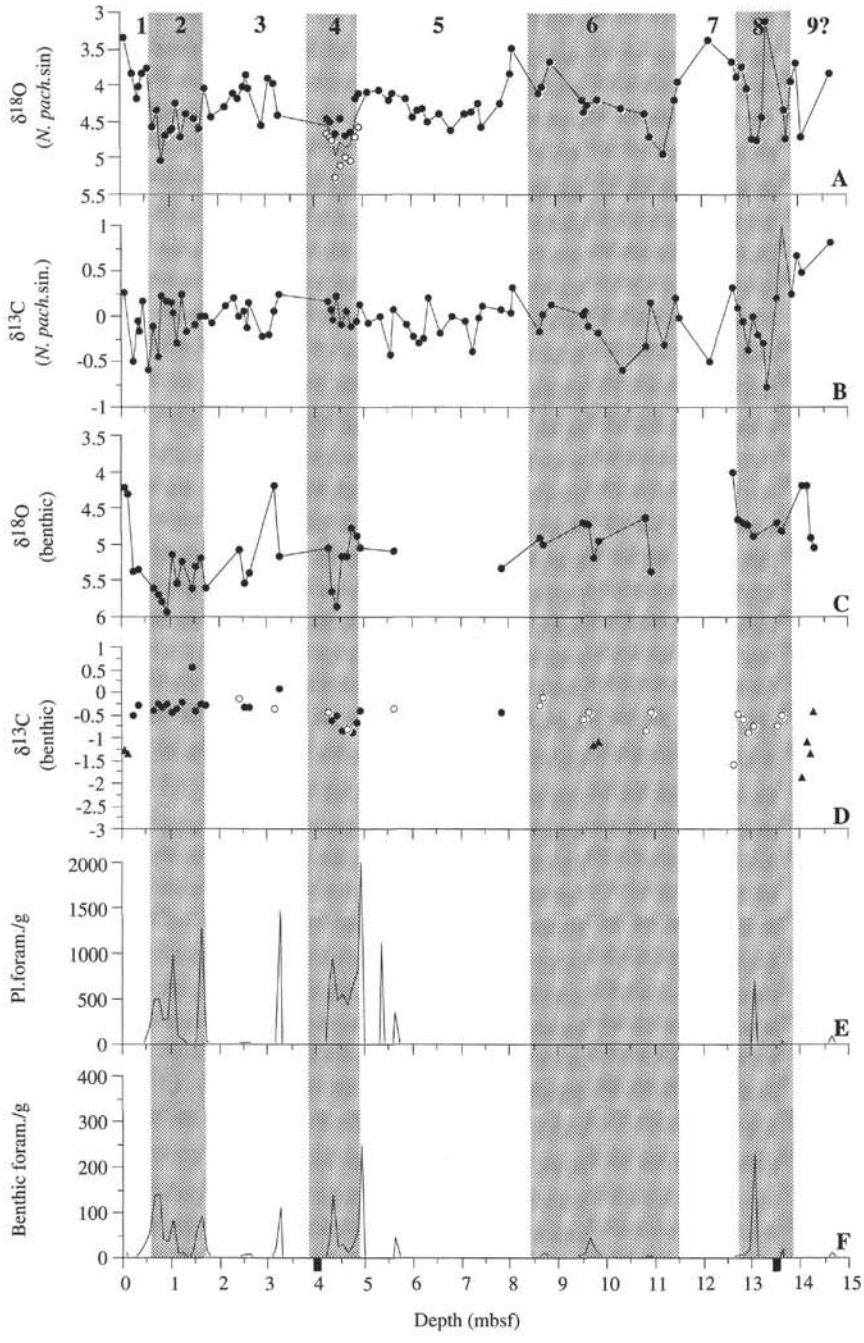

Figure 5. Isotope records in per thousand (‰) vs. PDB, and biogenous data from Hole 912A. The numbers of the isotope stages are on top, and the glacial stages are shaded. **A.** Planktonic $\delta^{18}O$ record measured on *N. pachyderma* (sinistrally coiling). **B.** Planktonic $\delta^{13}C$ record measured on *N. pachyderma* (sinistrally coiling). Double measurements are shown by both open and solid circles in (A) and (B). **C.** Benthic $\delta^{18}O$ record measured on *C. teretis,* and on *I. nocrossa* and *N. barleeanum,* which were corrected –0.25‰ and +0.16‰, respectively. **D.** Benthic $\delta^{13}C$ record measured on *C. teretis* (open circles), *I. nocrossa* (solid circles), and *N. barleanum* (triangles). **E.** Content of planktonic foraminifers per gram of dry sediment, based on counts in the >150-µm fraction. **F.** Content of benthic foraminifers per gram of dry sediment, based on counts in the >150-µm fraction. Black bars on depth scale indicate core breaks.

and temperature. The absolute $\delta^{18}O$ values are about 1‰ higher in the benthic record than in the planktonic. This may be caused by differences in the isotope composition of surface and deep water and/or by differences in temperature. If we employ the 0.4‰ deviation from equilibrium for *N. pachyderma* (sinistrally coiling) proposed by Johannessen (1992) and subtract the planktonic/benthic oxygen isotope gradient by this amount, the surface/deep-water temperature gradient was in general only a few degrees during the growth season of *N. pachyderma.* Carbon isotopes exhibit frequent variability throughout the record and within each isotope stage, and there is little covariance between the carbon and oxygen isotopes. Peaks of light planktonic $\delta^{18}O$ values are a common feature through the record, both in "cold" and "warm" isotope stages, with the most prominent peak occurring in Stage 8. This probably reflects periods of low salinity in the surface water, mainly caused by the melting of icebergs or meltwater runoff from the adjacent continent. Stage 6 has relatively light $\delta^{18}O$ values through most of the period, which may be an indication of high deglacial sedimentation rates or that the upper heavy substage of Stage 6 is missing due to sample spacing/resolution. These features are not clearly shown in the benthic record and may be explained by low resolution or by the fact that some low salinity/meltwater events were not transmitted from surface to deep water. The interglacials and the warmer periods mainly have $\delta^{18}O$ values below 4.5‰. Stage 9 is an exception, having variabilities in $\delta^{18}O$ from interglacial to glacial values, but there are some uncertainties concerning the boundaries of this stage.

Foraminifers are most common in the upper parts of the core; below 6 m they are sporadic and are present in very small amounts in

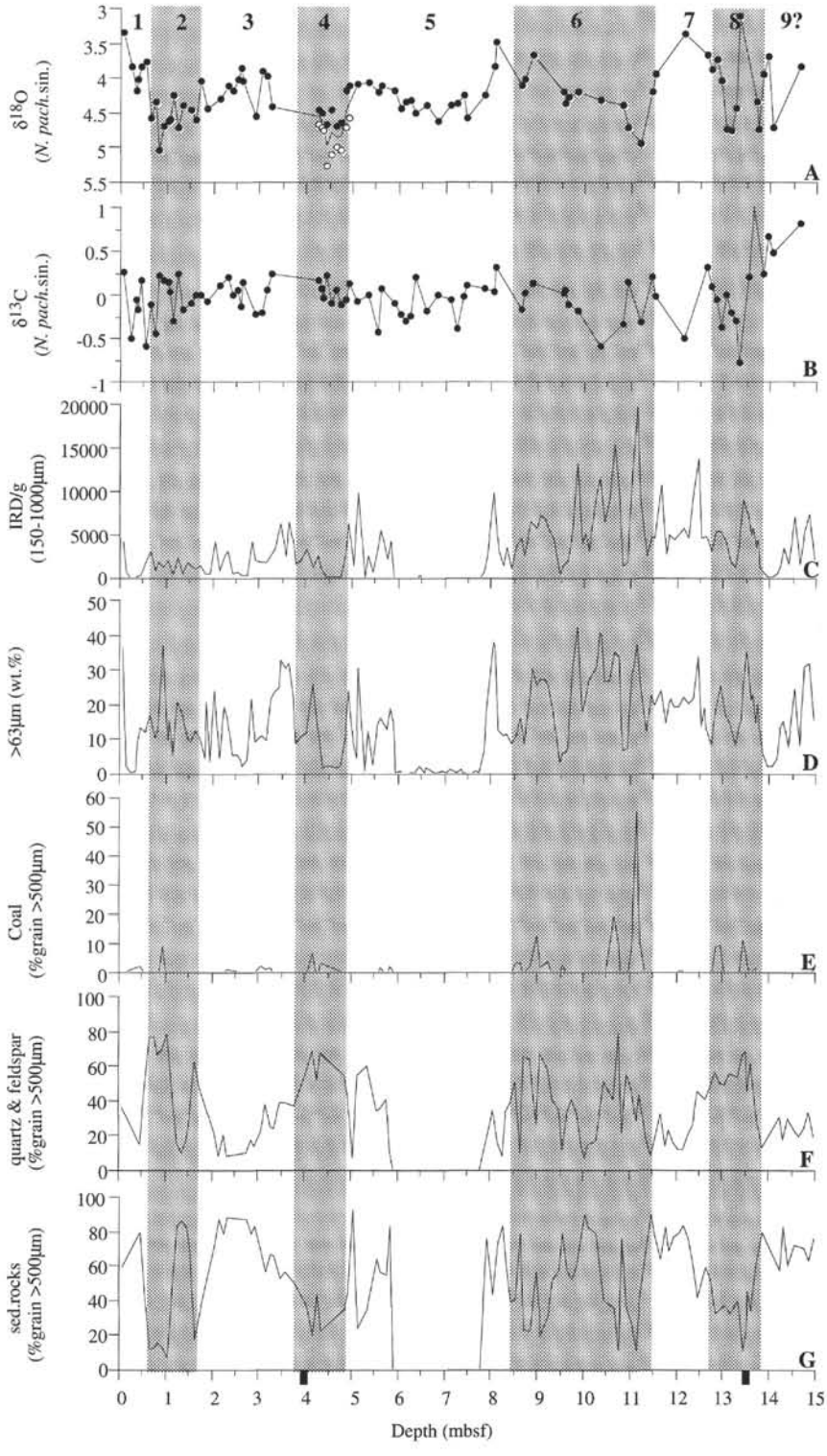

Figure 6. Planktonic isotopes in per thousand (‰) vs. PDB, and sedimentological data from Hole 912A. The numbers of the isotope stages are on top, and the cold stages are shaded. **A.** Planktonic $\delta^{18}O$ record measured on *N. pachyderma* (sinistrally coiling). **B.** Planktonic $\delta^{13}C$ record measured on *N. pachyderma* (sinistrally coiling). Double measurements are shown by both open and solid circles in (A) and (B). **C.** IRD content per gram of dry sediment, based on counts in the >150-µm fraction. **D.** Grain size (wt% >63 µm). **E.** Coal content in relative percentages, based on counts in the >500-µm fraction. **F.** Content of monocrystalline rock fragments in relative percentages, based on counts in the >500-µm fraction. **G.** Content of sedimentary rock fragments in relative percentages, based on counts in the >500-µm fraction. Black bars on depth scale indicate core breaks.

each sample (Fig. 8E, F). The glacial Stages 2, 4, and 8 have the highest content of both planktonic and benthic foraminifers, and interglacial/interstadial stages have distinctly fewer foraminifers. This will be discussed later.

IRD and Sediment Analysis

As shown in Figure 6C, the amount of IRD >150 µm is higher during earlier glaciations than during the last one. The same pattern was evident in Hole 909B and appears to be a regional phenomenon. The IRD content is high both in glacial and interglacial periods at Site 912, except in Stage 5, unlike in Hole 909B, where interglacials have a very low IRD content . The highest IRD content occurs in Stage 6, varying from less than 1000 to almost 20,000 grains per gram, indicative of a large iceberg flux. There also is a significant content of coarse-grained material in parts of the interglacial Stages 5, 7, and 9 (Fig. 6C, D). Some of this can be the result of ice rafting continuing into the interglacial stage. The relatively high content of coarse ma-

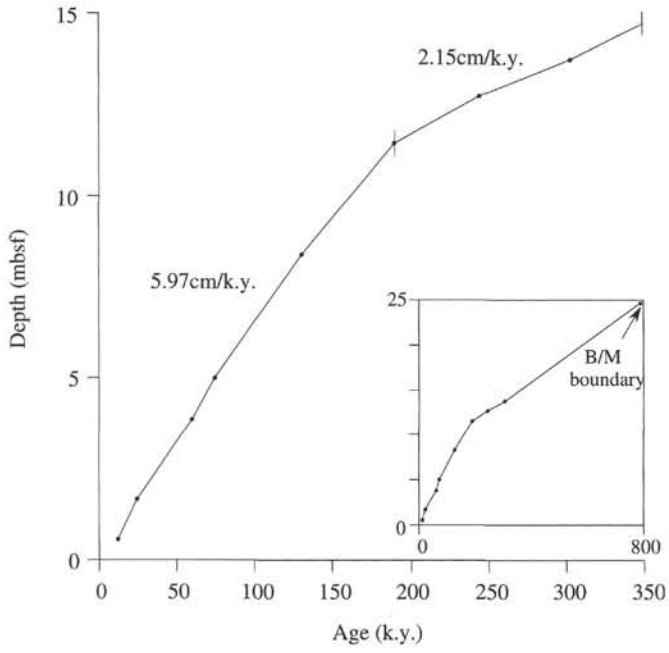

Figure 7. Average sedimentation rates in Hole 912A for the isotope stages during the last 500 k.y. Sedimentation rates extending to the Brunhes/Matuyama boundary are incorporated (Myhre, Thiede, Firth, et al., 1995).

terial throughout the core may also be explained by the location on the continental slope and the proximity to land, unlike Hole 909B, which is located in the central Fram Strait. In the middle of Stage 5, there is a 2-m interval with no coarse fraction content at all (Fig. 6C, D). This represents a distinct change in sedimentation that is not observed elsewhere in the studied section. Glacial stages, particularly Stage 6, are marked by a high coal content. Minor amounts of coal are also observed in Stages 4 and 2. Thus, coal occurrence appears to be mainly a glacial phenomenon, having its highest occurrence during large glaciations when there is a high input of IRD (also shown in Hole 909B). Monocrystalline fragments dominate during cold periods when there is a high input of IRD, whereas sedimentary rocks are most abundant in warmer periods (Fig. 6F, G). This may indicate different circulation patterns and variations in the source regions for the IRD.

DISCUSSION

Paleoenvironments of Isotope Stage 6–12

Glacial Variations

From analysis of the petrographic composition of coal in isotope Stage 6 in cores from the Fram Strait, Bischof et al. (1990) found northern Siberia as the most likely source area for the coal. We suggest that this is the same for the coal found in Stage 6 in Holes 909B and 912A. Low percentages of sedimentary rock fragments, which most likely originate from the Svalbard region, in the intervals containing coal also indicate that the coal is not of Svalbard origin because a high abundance of such rock fragments would be expected to accompany Svalbard coal. In Hole 909B, the same inverse coal/sedimentary rock fragment relationship as in Stage 6 is also apparent for glacial Stages 8, 10, and 12. As the IRD pattern for the older glaciations is the same, we propose that the source area for coal was the same during these glaciations. The content of coal during the last glaciation is very small and may be caused by a smaller extent of the Siberian glaciers during the Weichselian than in earlier glacials.

In isotope Stages 10(?) and 12,(?) there are several large fluctuations in IRD content, with increasing magnitude toward the end of the glaciations. These IRD peaks are dominated by coal, quartz, and feldspar (Fig. 3C, D, G) and are probably caused by large fluctuations in the continental ice sheets. In order to supply the IRD, there must be an ice advance that allows the submission of calving icebergs into the ocean. There are four such large ice advances during Stage 12 and three in Stage 10, with the largest IRD input in late Stage 10 following the peak glaciation indicated by the heaviest planktonic $\delta^{18}O$ signal. Isotope Stage 8 has the lowest IRD content of the pre-Stage 5 glaciations in both Hole 909B and 912A. This is also a less extreme gla-

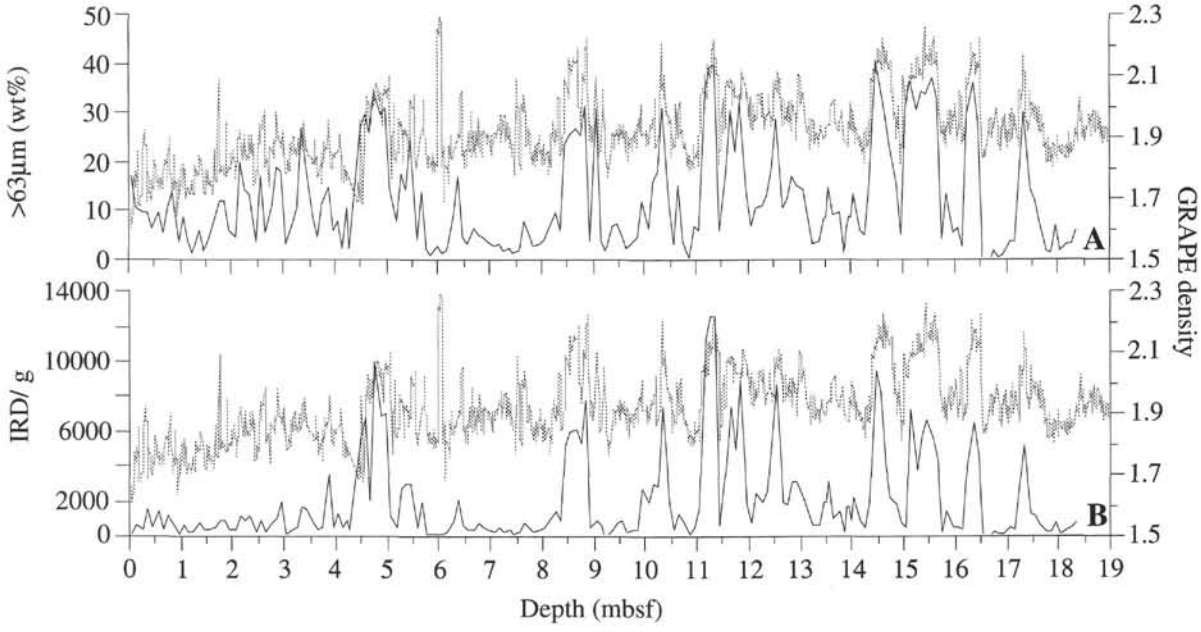

Figure 8. Comparison of the GRAPE density and (**A**) the weight percentage >63 µm and (**B**) the counted IRD >150 µm, presented as a number per gram of dry sediment in Hole 909B.

cial in the global isotope record (Shackleton and Opdyke, 1973). In Hole 912A, Stage 6 shows an opposite trend compared to Hole 909B, with the heaviest planktonic $\delta^{18}O$ values and highest content of IRD and coal observed in early Stage 6. Also, the peaks in IRD and coal decrease in size toward the end.

In both cores, the interglacial Stage 9 has an internal IRD peak of about the same magnitude as in glacial Stage 8. The peak has, however, a very different composition of the 500-μm fraction than in the glacial stages. The sedimentary rock fragments are dominating in Stage 9, indicating Svalbard as the most likely source area for the IRD, whereas Stage 8 is more dominated by the coal, quartz/feldspar type of IRD, with possible origins in Siberia. This appears to be a general phenomenon, where IRD from interglacial/interstadial stages in general are different from the glacial stages and contain a larger proportion of fragments with probable origin in the Svalbard area, as documented in a detailed study of Spielhagen (1990). This indicates that glaciations of more local scope are the case in warmer stages or during initiation of glaciation.

Surface Circulation

Glacial stages contain more foraminifers than interglacials, with maximum foraminifer abundance occurring between the IRD/coal peaks. This puzzling observation is consistent with more detailed studies of IRD/foraminifer relationships for the last glacial (Stages 2 and 4) by Dokken (1995) and Fronval et al. (1995), which show a series of foraminifer abundance maxima interbedded with IRD peaks in the Nordic Seas, in a fashion similar to Heinrich layer cycles in the North Atlantic. The most apparent conclusion from our study is that this style is a common feature, especially of the younger glacials dating back to Stage 12. It appears to reflect a close coupling of iceberg discharges from the Eurasian ice sheets immediately followed by open-water conditions that support foraminifer productivity. It is apparent from studies of the modern foraminifer distribution that permanent sea-ice cover results in low foraminifer content in the sediments (Johannessen et al., 1994). Hence, the high foraminifer content indicates open waters either in the form of persistent polynias or, more likely, a result of advances of Atlantic waters as far north as the Fram Strait/Yermak region after deglaciation events of the glacials. This indicates a very dynamic role for the surface circulation of the Nordic Seas during ice buildup and decay, probably closely coupled with large instabilities of the high-latitude ice sheets. The heat release from the seasonally open ocean and the latent heat from the resulting precipitation could potentially provide negative feedback to ice growth. Apparently, this is not enough to counteract the positive effect of increased moisture on ice growth. Because the foraminifer rich zones come after the IRD peaks, it does not appear as if the heat increase led to the deglaciations, which rather appear to take place within cold intervals (Fronval et al., 1995; Dokken, 1995).

The lower foraminiferal content in interglacials, as particularly seen in Hole 912A (Fig. 5) is most likely a result of dissolution and low carbonate production. Carbonate dissolution is widespread on the shelf and slopes around the Barents Sea (Steinsund and Hald, 1994), resulting from the production of corrosive brines on the shelf that may cascade down the slope as density-driven currents and also produce dissolution at greater depths on the margin. Because the shelf areas were smaller due to eustatic lowering and with periodic ice-sheet cover, this process was probably less important during glacials.

The lower foraminifer content in interglacials in Hole 909B cannot be explained by this mechanism. The site is located away from the margins in the deep Fram Strait, which is connected without restrictions to deep waters of the Nordic Seas. If corrosive interglacial deep waters were important in the Fram Strait, they should be important elsewhere as well. Carbonate and foraminifer abundance records further south do not support this, however, and we conclude that the low foraminiferal content in Hole 909B is a reflection of lower foraminifer productivity (i.e., a more persistent sea-ice cover).

In general, the foraminifer content appears to increase upcore, indicating that the system of open waters within glaciations is developing and is most pronounced during the last two glacial cycles.

Deep Water

The quite close correspondence between the planktonic and benthic $\delta^{13}C$ records in Hole 909B indicates that there is communication between the surface and deep water through most of the record. Below Stage 9, there are very few benthic isotope measurements, but where they exist they show the same pattern. In Hole 912A, there is little coherency between the planktonic and benthic $\delta^{13}C$ records, probably because bottom waters on the Svalbard margin are formed at times by shelf processes and are influenced by carbon cycling on the shelf.

Paleoenvironments of Isotope Stage 5

Glaciation Record

The onset of isotope Stage 5 is marked by a light $\delta^{18}O$ peak occurring simultaneously with an IRD peak. This is most clearly shown in Hole 912A and indicates an overprint of meltwater at Termination II, culminating in early Stage 5e. This is also found at the Vøring Plateau and the Iceland Plateau (T. Fronval, pers. comm., 1995). The first part of Stage 5e might be lost in the core break in Hole 909B, and, therefore, the meltwater signal is not clearly shown in this record. At Hole 912A, Substage 5d is followed by an increased amount of IRD occurring simultaneously with lighter $\delta^{18}O$ values, probably as a result of a deglacial phase on Svalbard at the 5d/5c transition. Terrestrial data also indicate considerable ice-sheet growth on Svalbard during 5d (Mangerud and Svendsen, 1992). Hebbeln (1992) did not find evidence for any increased ice rafting in the central Fram Strait during Stage 5, but the Hole 909B data and the data presented by Dokken (1995) indicate a glacial advance probably reaching the inner shelf area with a transport of icebergs westward to the central Fram Strait.

The IRD data from Hole 912A give a totally different picture. In mid-Stage 5, there is an interval with no coarse fraction at all (i.e., no IRD), indicating the rapid sedimentation of fines. This can also be seen in the data of Hebbeln (1992) from the same area, showing the lowest input of coarse-grained material in the cores close to the shelf or at the continental slope. A possible explanation is that the northernmost parts of the Fram Strait and/or the shelf area around northern Svalbard were covered by sea ice during this period and that fine sediments were deposited under the ice. If so, melting of icebergs during/after Stage 5d did not occur this far north, and ice rafting can, therefore, only be observed further south on the shelf and in the central Fram Strait.

Stage 5a is marked by a shift toward lighter planktonic $\delta^{18}O$ values in both holes, also recognized by Köhler and Spielhagen (1990). In Hole 912A, this shift corresponds with an increased input of IRD, contrary to Hole 909B, where the IRD content slightly decreases. The difference in IRD deposition between the two sites may be the result of a northward surface current transporting icebergs in a narrow "belt" along the coast or because most of the melting occurred at the shelf and slope instead of reaching the central parts of the Fram Strait.

Surface- and Deep-Water Paleoceanography

The $\delta^{18}O$ values in Stage 5e are close to modern values. Due to possible influence of low salinities in this kind of environment, it is difficult to extract temperature information from the $\delta^{18}O$ values. It is also difficult to assess the SSTs of Stage 5e due to the low resolution and low foraminifer content in Hole 912A and the possible missing

interval at the core break in Hole 909B. There is a tendency for planktonic $\delta^{13}C$ values in 909B to be lighter in the "warm" substages of isotope Stage 5 than in 5d and 5b. Using the present distribution of planktonic $\delta^{13}C$ in the Nordic Seas (Johannessen et al., 1994), where Atlantic waters are more negative than Arctic water, this can be viewed as a higher influx of Atlantic water in Substages 5e, 5c, and 5a and more Arctic water in 5d and 5b.

The different IRD records in Stage 5 at the two sites may be due to the current pattern and/or sea-ice cover, which prevented icebergs from drifting to the Yermak Plateau during Substage 5d to 5b. In Hole 909B, planktonic and benthic foraminifers are present in the "warmer" periods of Stage 5, thus, as there is a very low foraminifer content during this period in Hole 912A, favoring this assumption. The low foraminifer content in Hole 912A in Stage 5 may also be due to dilution by high nonbiogenic sedimentation and dissolution from corrosive brines. Stage 5a exhibits much lighter $\delta^{18}O$ values than the rest of Stage 5. In Hole 909B, it almost reaches present values, and foraminifers are present in high amounts, indicating a strong influx of warm Atlantic water, also shown in data from Gard and Backman (1990) and Köhler and Spielhagen (1990). The low amount of IRD in Hole 909B in Substage 5a can be explained by a northward current transporting icebergs along western Svalbard, not reaching the position of Site 909 further west in the Fram Strait. The dominance of sedimentary rock fragments in the warmer periods supports these interpretations, assuming that most of these originate from Svalbard and the Barents Sea. During open-water conditions, there is a northward surface circulation along the coast of Spitsbergen that transports icebergs with sedimentary rocks from the (eastern) Svalbard/Barents Sea area. This is most clearly shown in Hole 909B, where sedimentary rocks are dominant in most parts of Stage 5 and, therefore, most likely reflect open-water conditions in the central Fram Strait through most of this period. During Stage 5a, monocrystalline rock fragments dominate, possibly indicating a source area other than Svalbard (possibly Scandinavia), with IRD transported northward with Atlantic water masses.

Based on the good coherency between planktonic and benthic $\delta^{13}C$ values in Hole 909B (Fig. 2B, C), we assume that deep water was formed in the Nordic Seas throughout isotope Stage 5.

Paleoenvironments of Isotope Stages 1–4

Glaciation Record

The transition from Stage 4 to 5 is clearly shown by the increase in $\delta^{18}O$ values. The low $\delta^{18}O$ values through most of the period probably reflect the growing continental ice sheets, but some meltwater/low-salinity influence is apparent in Hole 909B. The IRD content is low in the middle part of Stage 4, possibly because this is an ice-growth phase with less calving than in a deglaciation phase after an ice-sheet culmination. The increased IRD content at the end of the stage indicates increased calving as the glaciers reach the coast and can be correlated to other cores in the Fram Strait (Hebbeln, 1992) and to terrestrial data (Mangerud and Svendsen, 1992).

The disintegration of the ice sheet culminates in a distinct meltwater pulse in early Stage 3 as shown by the very low $\delta^{18}O$ and $\delta^{13}C$ values (Fig. 3A, B) and an IRD peak (Fig. 6C). This strong component of meltwater is suggested by Dokken (1995) to represent the melting of an ice sheet that covered major parts of the shelf areas, including the Barents Sea, during Stage 4. Influence from meltwater, indicated in the spiky $\delta^{18}O$ (and $\delta^{13}C$) records, is a pronounced feature through Stage 3 and is also documented in cores further south (Fronval et al., 1995; Vogelsang, 1990). This can probably be related to smaller ice advances that at least reach the fjords. The meltwater pulses are not associated with a marked increase in IRD content in Hole 909B (Fig. 3), unlike the situation in Hole 912A (Fig. 6), where ice rafting seems to be relatively high through most of the stage. This can again reflect the transport of ice northward in a relatively narrow zone along the west coast of Svalbard. Stage 2 is clearly recognized by the high $\delta^{18}O$ values reflecting the glaciation maximum. The IRD content is relatively low during this period, which may be the result of a growing ice sheet with little meltwater and iceberg production. Some light $\delta^{18}O$ peaks probably indicate some melting, just before and after the maximum glaciation, but they are not paralleled by a significant increase in IRD input. Melting of the Weichselian ice sheet is shown by a light $\delta^{18}O$ signal at the transition to Stage 1. Only the initial melting is present in Hole 909B. In Hole 912A, two meltwater pulses are recognized. A significant increase in IRD parallels this meltwater signal.

Surface- and Deep-Water Paleoceanography

High foraminifer content during Stages 2 and 4 indicates periods with seasonal open-water conditions with an influx of Atlantic water all the way north to the Yermak Plateau. These periods also have a dominance of monocrystalline rock fragments, probably pointing to source area other than Svalbard. Most likely, these fragments originate from Scandinavia (and/or Great Britain) and were transported northward with the Atlantic water masses. The intervals that contain no foraminifers show a dominance of sedimentary rocks, probably with the Svalbard/Barents Sea region as the source area. During Stage 3, there is a dominance of sedimentary rock fragments throughout the period. This can be connected to the breakup of glaciations on Svalbard and the Barents Sea shelf with little input of ice-rafted material from other sources. The same is shown in Stage 1 with a dominance of sedimentary rocks during the initial melting, and then a slight increase in the amount of crystalline rocks that occurs simultaneously with a decrease in $\delta^{18}O$ values in the uppermost sample, indicating a stronger influx of water masses from the south.

Formation of deep water in the Nordic Seas seems to be continuous from Stage 1 to 4, inferred from the parallel planktonic and benthic $\delta^{13}C$ records. Bottom water formed in the Arctic Ocean and/or the Barents Sea may flow over the Yermak Plateau, especially during "warmer" periods when brine formation occurs at the shelf areas.

Long-Term Evolution of Glaciations

Figures 8 and 9 show a very close coherency between the gamma-ray attenuation porosity evaluator (GRAPE) density record measured on the shipboard multisensor track unit and the coarse fraction (wt% >63 μm) and the IRD records (>150 μm) in both Holes 909B and 912A (data from Myhre, Thiede, Firth, et al., 1995). The >63-μm fraction has less variations in amplitude than the IRD record and gives a more one-to-one coherency with the GRAPE density record. The good correlation between the GRAPE density and the coarse fraction/IRD is most clearly shown in Hole 909B, where every major peak in the IRD record is associated with an increase in GRAPE density. Based on this, we assume that the GRAPE density record is a good proxy for the coarse fraction and the IRD input further back in time than our detailed studies go (Figs. 10, 11). The record in Hole 909B shows large amplitudes in the IRD and documents clear differences between interglacial and glacial periods. Because the IRD record is mimicked by GRAPE measurements, the GRAPE data can be interpreted as a signal of glacial/interglacial variability further downhole.

The age model for Hole 909B (Fig. 12A) indicates continuous sedimentation over the past 2 m.y. Before the Jaramillo Subchron, sedimentation rates were higher than during the Brunhes Chron. There is a change in the GRAPE density record in the early Brunhes, at about 33 mbsf (~0.7 Ma), toward more prominent peaks of high GRAPE density. This is probably connected with a transition to more severe glaciations with stronger IRD flux. Whether this reflects the shift of climatic response from the dominant 41 k.y. tilt cycle of the Matuyama to the dominant 100 k.y. power in the Brunhes is hard to tell. However, the variation in the GRAPE record seems to be less

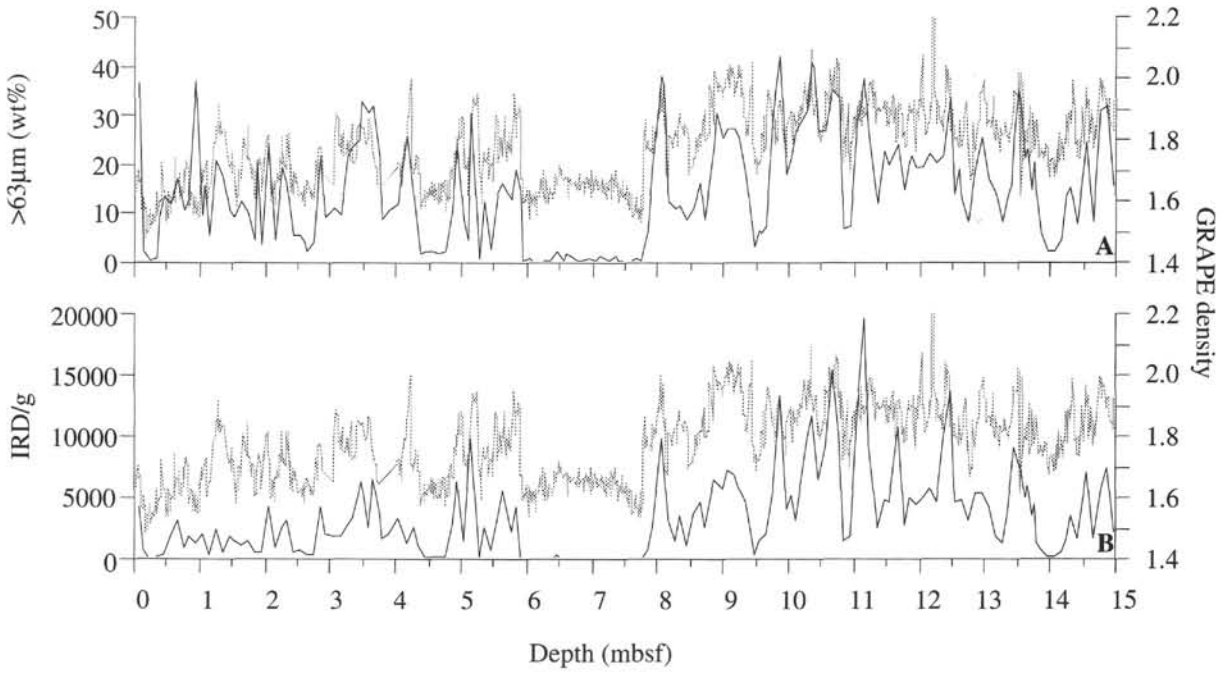

Figure 9. Comparison of the GRAPE density and (**A**) the weight percentage >63 µm and (**B**) the counted IRD >150 µm, presented as number per gram of dry sediment in Hole 912A.

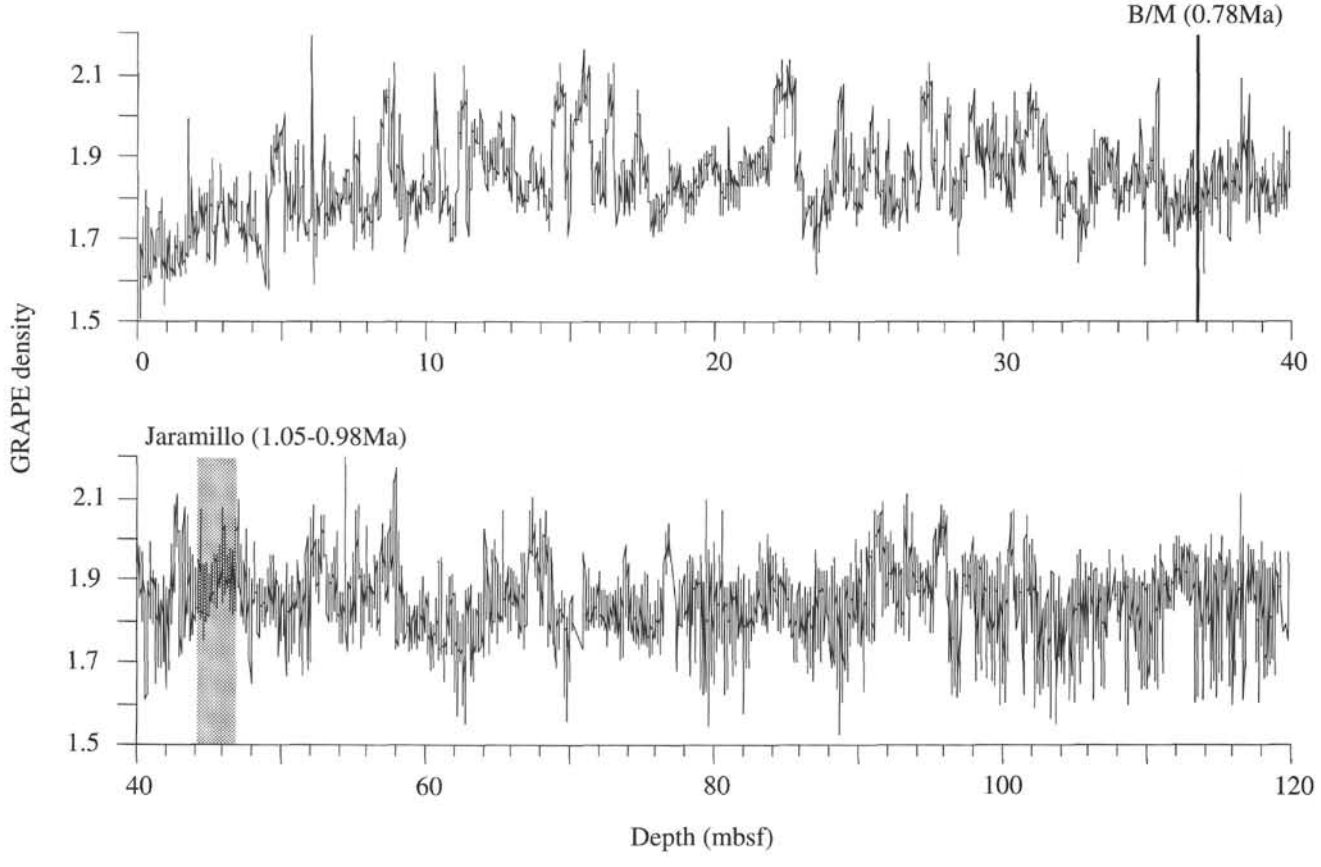

Figure 10. GRAPE density record for the upper 120 m of Hole 909B. Magnetic reversal boundaries are indicated (Myhre, Thiede, Firth, et al., 1995).

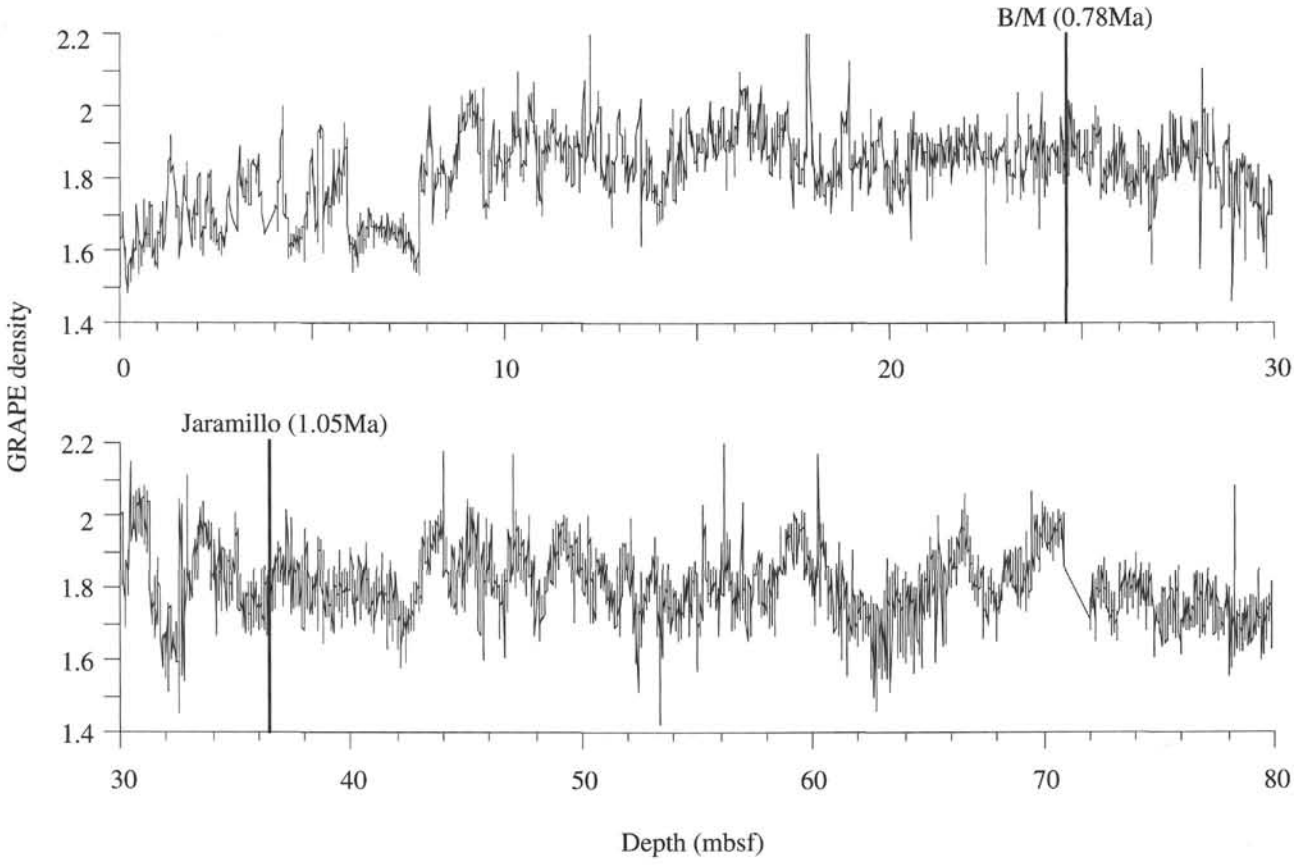

Figure 11. GRAPE density record for the upper 80 m of Hole 912A. Magnetic reversal boundaries are indicated (Myhre, Thiede, Firth, et al., 1995).

dramatic in the pre-Brunhes period than after the shift in the early Brunhes.

In Hole 912A, there is probably a hiatus or condensed section within the Brunhes Chron as evidenced by the low sedimentation rates from the Brunhes/Matuyama boundary up to 15 mbsf, but the sedimentation rates are also low during the period from the Jaramillo to the Brunhes/Matuyama boundary (Fig. 12B). Similar to that in Hole 909B, there is a change in the GRAPE record in the early Brunhes Chron, but unlike that in Hole 909B, there are some large fluctuations just after the Jaramillo Subchron. The pre-Jaramillo period has sedimentation rates twice as high as the post-Jaramillo in Hole 912A (Fig. 12B), and there are equally large fluctuations in the GRAPE density record here as above 20 mbsf. This can be due to more pronounced erosion and deposition that affects the margin site more than the one in the central Fram Strait, and both GRAPE density and sedimentation rates thus indicate large-scale erosion in the European Arctic during the Matuyama with 41-k.y. cyclicity dominating the global ice-volume record. The higher sedimentation rates prior to the Brunhes agree with evidence from the Bear Island Fan that sedimentation rates were two to four times higher during this period than during the late Pleistocene (Laberg and Vorren, in press). The total dominance of 41-k.y. cycles in global ice-volume records in the Matuyama may indicate ice-sheet fluctuations more confined to the high latitudes than in the late Quaternary because the 41-k.y. influence on insolation is strongest at high latitudes. Although time series studies have to document the frequency pattern of IRD/glacial activity during the Matuyama, the evidence from Hole 912A indicates that high-latitude glaciation indeed was important during the Matuyama.

CONCLUSIONS

The main features in the paleoenvironmental evolution during the last 300 k.y. are similar in the records from the Fram Strait and the Yermak Plateau. Earlier glaciations (isotope Stages 6–12) were more severe than the last one, as shown by a higher IRD flux and the appearance of Siberian coal in IRD peaks. The content of foraminifers through time indicates a trend toward more open water, with a higher production during the two last glacial/interglacial cycles. Seasonal open-water conditions with a high foraminifer production occurred through all the glacial periods, indicating that the surface circulation of the Nordic Seas in glacial stages plays an important role in the growth and decay of high-latitude ice sheets, bringing moisture and heat northward also in the glacials. Deep-water formation seems to be continuous in the Nordic Seas through most of the period presented in this study, as shown by the parallel planktonic and benthic $\delta^{13}C$ record in Hole 909B. There was an apparent change in the style of glaciation in the earlier parts of the Brunhes Chron with the emergence of more strongly developed IRD peaks than before. Strong glacial activity is an important element also in the Matuyama Chron in the European Arctic.

ACKNOWLEDGMENTS

We thank Odd Hansen and Rune Søraas for mass spectrometer operation and Else Loodtz for help with the manuscript. Reviews by Ralph Thiedemann and Tore Vorren were very helpful. This study

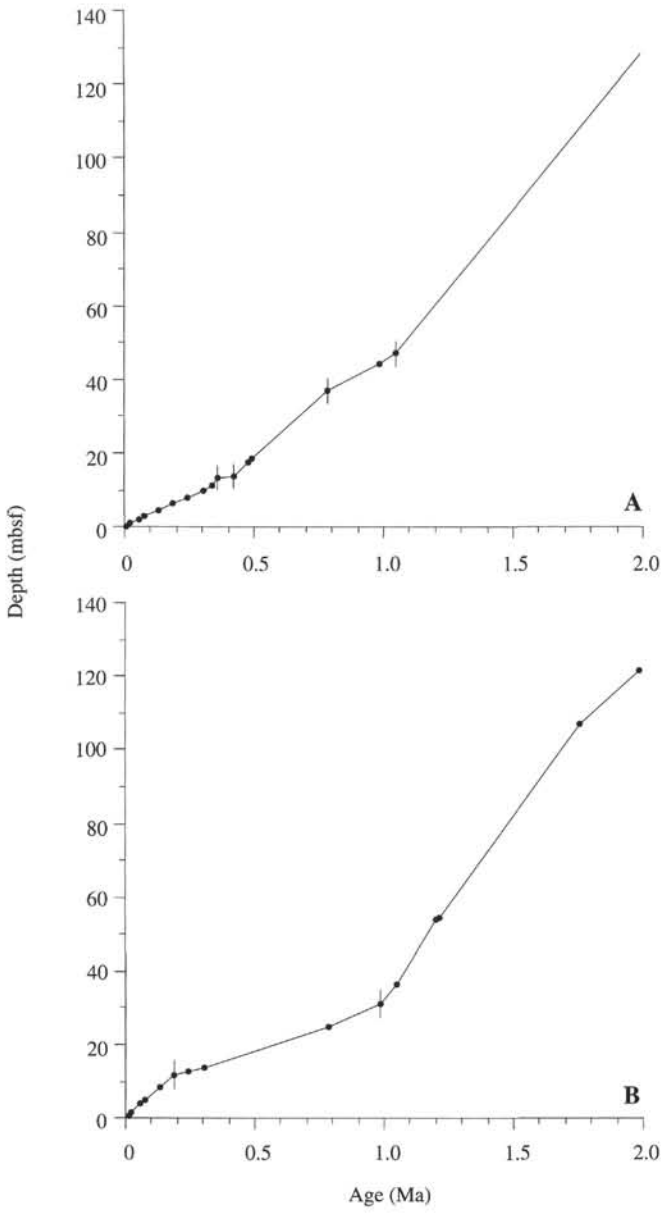

Figure 12. Average sedimentation rates for the last 2 m.y., based on the the isotope stratigraphy for the upper part and the paleomagnetic record for the lower part (Myhre, Thiede, Firth, et al., 1995). **A.** Sedimentation rates for Hole 909B. **B.** Sedimentation rates for Hole 912A.

was supported by the Norwegian Research Council (NFR) and the Norwegian Petroleum Directorate (NPD).

REFERENCES

Bischof, J., Koch, J., Kubisch, M., Spielhagen, R.F., and Thiede, J., 1990. Nordic Seas surface ice-drift reconstructions: evidence from ice-rafted coal fragments during oxygen isotope stage 6. *In* Dowdeswell, J.A., and Scourse, J.D. (Eds.), *Glacimarine Environments: Processes and Sediments.* Geol. Soc. Spec. Publ. London, 53:235–251.

CLIMAP Project Members, 1976. The surface of the ice-age Earth. *Science,* 191:1131–1137.

Dokken, T.M., 1995. Paleoceanographic changes during the last interglacial-glacial cycle from the Svalbard-Barents Sea margin: implications for ice-sheet growth and decay [Doctor Scientarium thesis], Univ. of Tromsø.

Fronval, T., Jansen, E., Bloemendal, J., and Johnsen, S., 1995. Oceanic evidence for coherent fluctuations in Fennoscandian and Laurentide ice sheets on millennium timescales. *Nature,* 374:443–446.

Gard, G., and Backman, J., 1990. Synthesis of arctic and subarctic coccolith biochronology and history of North Atlantic Drift water influx during the last 500,000 years. *In* Bleil, U., and Thiede, J. (Eds.), *The History of the Polar Oceans: Arctic Versus Antarctic:* Dordrecht (Kluwer), 499–518.

Graham, D.W., Corliss, B.H., Bender, M.L., and Keigwin, L.D., Jr., 1981. Carbon and oxygen isotopic disequilibria of Recent deep-sea benthic foraminifera. *Mar. Micropaleontol.,* 6:483–497.

Haake, F.W., and Pflaumann, U., 1989. Late Pleistocene foraminiferal stratigraphy on the Vøring Plateau, Norwegian Sea. *Boreas,* 18:343–356.

Hebbeln, D., 1992. Weichselian glacial history of the Svalbard area: correlating the marine and terrestrial records. *Boreas,* 21:295–304.

Hebbeln, D., Dokken, T., Andersen, E.S., Hald, M., and Elverhøi, A., 1994. Moisture supply for northern ice-sheet growth during the Last Glacial Maximum. *Nature,* 370:357–360.

Hebbeln, D., and Wefer, G., 1991. Effects of ice coverage and ice-rafted material on sedimentation in the Fram Strait. *Nature,* 350:409–411.

Jansen, E., and Sejrup, H.P., 1987. Stable isotope stratigraphy and amino-acid epimerization for the last 2.4 m.y. at Site 610, Holes 610 and 610A. *In* Ruddiman, W.F., Kidd, R.B., Thomas, E., et al., *Init. Repts. DSDP,* 94 (Pt. 2): Washington (U.S. Govt. Printing Office), 879–888.

Johannessen, T., 1992. Stable isotopes as climatic indicators in ocean and lake sediments [Dr. scient. thesis]. Univ. of Bergen.

Johannessen, T., Jansen, E., Flatøy, A., and Ravelo, A.C., 1994. The relationship between surface water masses, oceanographic fronts and paleoclimatic proxies in surface sediments of the Greenland, Iceland Norwegian Seas. *In* Zahn, R., and Kaminski, M. (Eds.), *Carbon Cycling in the Glacial Ocean:* Heidelberg (Springer Verlag).

Kellogg, T.B., 1980. Paleoclimatology and paleo-oceanography of the Norwegian and Greenland seas: glacial/interglacial contrasts. *Boreas,* 9:115–137.

Köhler, S.E.I., and Spielhagen, R.F., 1990. The enigma of oxygen isotope stage 5 in the central Fram Strait. *In* Bleil, U., and Thiede, J. (Eds.), *The History of the Polar Oceans: Arctic versus Antarctic:* Dordrecht (Kluwer), 489–497.

Laberg, J.S., and Vorren, T.O., in press. The middle and late Pleistocene evolution of the Bear Island Trough Mouth Fan. *Global Planet. Change.*

Mangerud, J., and Svendsen, J.I., 1992. The last interglacial-glacial period on Spitsbergen, Svalbard. *Quat. Sci. Rev.,*11:633–664.

Martinson, D.G., Pisias, N.G., Hays, J.D., Imbrie, J., Moore, T.C., Jr., and Shackleton, N.J., 1987. Age dating and the orbital theory of the ice ages: development of a high-resolution 0 to 300,000-year chronostratigraphy. *Quat. Res.,* 27:1–29.

Myhre, A.M., Thiede, J., Firth, J.V., et al., 1995. *Proc. ODP, Init. Repts.,* 151: College Station, TX (Ocean Drilling Program).

Poole, D.A.R., Dokken, T.M., Hald, M., and Polyak, L., in press. Stable isotope fractionation in recent benthic foraminifera from the Barents and the Kara Seas. *Paleoceanography.*

Shackleton, N.J., and Opdyke, N.D., 1973. Oxygen isotope and paleomagnetic stratigraphy of equatorial Pacific core V28-238: oxygen isotope temperatures and ice volumes on a 10^5 year and 10^6 year scale. *Quat. Res.,* 3:39–55.

Spielhagen, R.F., 1990. Die Eisdrift in der Fram Strasse während der letzten 200.000 Jahre [Ph.D. thesis]. Univ. of Kiel, *GEOMAR Rep.,* 4:1–133.

Steinsund, P.I., and Hald, M., 1994. Recent carbonate dissolution in the Barents Sea: paleoceanographic applications. *Mar. Geol.,* 117:303–316.

Vogelsang, E., 1990. Paläo-Ozeanographie des Europäischen Nordmeeres an Hand stabiler Kohlenstoff– und Sauerstoffisotope. *Ber. Sonderforschungsber. 313,* Univ. Kiel, 23:1–136.

Vorren, T.O., Vorren, K.D., Alm, T., Gulliksen, S., and Løvlie, R., 1988. The last deglaciation on Andøya, northern Norway. *Boreas,* 17:41–77.

Date of initial receipt: 7 July 1995
Date of acceptance: 30 December 1995
Ms 151SR-135